Density functional study of the polar MnO(111) surface

C. Franchini,* V. Bayer, and R. Podloucky
Institut für Physikalische Chemie, Universität Wien and Center for Computational Materials Science, Liechtensteinstrasse 22A, A-1090 Vienna, Austria

G. Parteder, S. Surnev, and F. P. Netzer
Institut für Experimentalphysik, Karl-Franzens-Universität Graz, Universitätsplatz 5, Graz A-8010, Austria
(Received 12 December 2005; revised manuscript received 17 February 2006; published 3 April 2006)

By application of a density functional approach within the PBE and PBE+U approximations we investigate the ground state terminations of the polar MnO(111) surface being in thermodynamic equilibrium with an oxygen reservoir. In the allowed range of the oxygen chemical potential and for realistic oxygen partial pressures the surface is found to undergo different structural transitions. In the oxygen-poor regime the most stable phases are the O- and Mn-terminated octopolar structures, which are almost degenerate in energy. For oxygen-rich conditions we observe a competition between the O-terminated unreconstructed bulk face and a *stripes* structure. We show that the stabilization of the polar surface in the thermodynamic equilibrium with the oxygen environment is due to remarkable changes of the geometrical structure (i.e., reconstruction and relaxation) and of the electronic structure (i.e., metallization).

DOI: 10.1103/PhysRevB.73.155402 PACS number(s): 68.35.Bs, 68.47.Gh, 73.20.At, 71.27.+a

I. INTRODUCTION

Metal oxide (MO) surfaces play a prominent role in a wide class of phenomena ranging from catalysis, electronics, digital storage, spintronics, and fundamental surface science. They comprise a very active field of research, both experimentally[1] and theoretically.[2] In particular, oxides crystallizing in the rocksalt structure (such as MgO, NiO, CoO, FeO, MnO) are intensively investigated. Among them, the electrostatically polar (111) surfaces have recently attracted more attention,[3–14] arising from the complexity to prepare defect free and unreconstructed surfaces and from the search for stabilization mechanisms for such polar surfaces. Although a large number of materials display polar surfaces in nature, the fundamental aspects of the processes favoring the neutralization of polarity remain one of the challenging issues of modern surface science. Several mechanisms have been proposed for the stabilization of polar surfaces,[2] namely by (1) the redistribution of the surface electronic structure, (2) changes in surface stoichiometry combined with structural changes such as reconstructions and terracing, (3) adsorption, hydroxylation, and the interaction with the residual atmosphere. However, a fundamental understanding of the phenomena responsible for the neutralization of polarity is still missing, and, most important, the theoretical investigation of the appearance of different phases of polar surfaces depending on external conditions (such as temperature and partial oxygen pressure) are rather scarce.[15–18]

The quantitative characterization of polar MO surfaces in terms of surface stoichiometry and morphology remains a difficult task for the usual experimental techniques (such as LEED, STM, SEM, REM, and RHEED), due to the insulating character of the substrate. Recently, grazing incidence x-ray scattering (GIXS) has overcome the limitations of standard techniques in treating charging effects. This method turned out to be an efficient analyzer of roughness, relaxation, and reconstruction of oxide surfaces, although for polar surfaces only a few results have been presented so far.[1] A further experimental limitation is due to the need of high-purity samples for an accurate atomistic description of MO surfaces. First principles calculations have become a powerful supplement to experimental techniques, providing reliable and accurate predictions of the structural and electronic properties of surfaces.

For polar surfaces with the rocksalt structure, extensive experimental and first principles studies have been performed on[3–7,13,19–28] MgO(111) and NiO(111),[6,8,10–12,14,29–36] CoO(111) (Refs. 14 and 37–39) and FeO(111).[14,40–43] In a simplified scheme, the (111) stacking of MO compounds with rocksalt structure consists of alternating layers of $M^{(+)}$ and $O^{(-)}$ ions which generate an electrostatic dipole field perpendicular to the surface. Following the classification of Tasker,[44] slabs modeling such (111) surfaces have a dipole moment which increases monotonically with the slab thickness, and therefore the surface energy also diverges as well with respect to the slab thickness.

The mechanism behind the cancellation of polarity for these (111) terminated surfaces has been studied in terms of reconstructions. Some of the morphologies proposed fulfill the electrostatic condition for neutrality (2×2 octopolar, 2×2 spinel, 2×1)[4,6,8,10,11,13,14,45] while others, involving the formation of cyclic ozone trimers [2×2, $(\sqrt{3}\times\sqrt{3})R30°$, $(2\sqrt{3}\times2\sqrt{3})R30°$] or derived from the octopolar structure (α reconstruction) do not trivially cancel the diverging electrical field within a standard ionic picture. Further chemical processes for stabilization have been claimed, which invoke the adsorption of transition metals[7,12] or the dissociative adsorption of water (H and OH).[3,6,28] Finally, Mori *et al.*[40] have recently proposed a new surface reconstruction, also derived from the octopolar structure, compatible with the surface ferromagnetism found in FeO(111).

Although MnO has gained much attention by both theory and experiment because of its fundamental properties (being

an intermediate Mott-Hubbard charge-transfer insulator[46]) and its technological importance (e.g., for catalysis, electronics, crystal growth), a deeper knowledge of its terminations, and in particular for the (111) surfaces, is almost absent.[47,48] The lack of experimental results has to be mainly ascribed to the difficulties in preparing MnO samples of good qualities. In the absence of experimental information capable to be compared to first principles study, theoreticians were discouraged to study the MnO(111) polar surface on a predictive level. Furthermore, standard density functional approaches are problematic because of the strong localization of the Mn states as expressed by large gaps and large magnetic moments. Nevertheless, the similarity with other (111) MO polar terminations boosts for an exploration of this surface. This is the aim of this study. Moreover, experimental studies on epitaxial thin film of MnO, which are presently on the way, provide a further impetus for our theoretical work.[49] In the present work we investigate the (111) polar surface of MnO. In particular, we focus our study on two basic questions, namely (1) are nonstoichiometric reconstructions responsible for polarity compensation as for MgO and NiO, and (2) which role does an oxygen environment play for the thermodynamic stability of the reconstructed surfaces.

From the computational point of view the investigation of a polar surface requires a special treatment which will be discussed in Sec. II, where the details on the *ab initio* technicalities are given. In Sec. III we present the types of reconstructions considered in our simulation. Section IV is devoted to the discussion of the results and contains information on the thermodynamical stability of the investigated structural models and the survey of the structural, electronic, and magnetic properties of the more favorable reconstructions. Section V concludes our findings.

II. COMPUTATIONAL ASPECTS

A. Methodology

The present first principles calculations were performed by utilizing the VASP (Vienna *ab initio* simulation package) program[50,51] within the generalized gradient spin density approximation (SGGA) to density functional theory (DFT) with the parameterization of Perdew, Burke, and Ernzerhof (PBE).[52] The calculations were carried out within the projector augmented wave (PAW) method[53] as implemented by Kresse and Joubert.[54] This is a frozen core method which uses the exact valence wave functions instead of nodeless pseudowave functions, as commonly applied for pseudopotentials calculations. The chosen valence electron configuration was $3d^6 4s^1$ and $2s^2 p^4$ for the Mn and O potentials, respectively. The kinetic energy cutoff for the plane wave basis set was 280 eV, which turned out to give sufficiently accurate results. Making use of the interatomic forces as derived from the Hellmann-Feynmann theorem, the atomic geometry was optimized until the change in total energy was smaller than 10^{-3} eV between two consecutive ionic configurations. During geometry relaxation a $5\times5\times1$ Monkhorst-Pack $\vec{k}$-point grid was used, whereas for the calculation of other ground state properties and the density of states (DOS) a refined $9\times9\times1$ $\vec{k}$-point mesh was considered.

Conventional SGGA is known to be inadequate to account for the electronic structure of materials with half filled *d* valence states. It is therefore necessary to use more sophisticated approaches[55] which properly take into account the on-site Coulomb repulsion. In this work we compare the results of standard SGGA (with PBE parameterization) with an[56] SGGA+U approach (PBE+U) implemented according to Dudarev.[57] In this approach, the parameters *U* and *J* do not enter independently, but only by the difference *U-J*. The value of $U\text{-}J=6.0$ eV and the lattice parameters of MnO ($a_{PBE}=4.37$ Å and $a_{PBE+U}=4.48$ Å) were taken over from our recent study on the phase of bulk MnO.[46]

To model the surface we used the finite-sized slab technique. The various supercells employed to explore the stability of different surface reconstructions are described in details in Sec. III. The computational treatment of polar surfaces requires special care, in particular to avoid the buildup of an overall artificial dipole field. The polarity is due to the $Mn^{(+)}/O^{(-)}$ sequence of the MnO slab which, being noncentrosymmetric, is O terminated on one side and Mn terminated on the other side when stoichiometry is maintained. Several schemes have been introduced to overcome this problem.[60,61] To suppress the charge transfer, we adopt a model with hydrogen atoms saturating the dangling bonds of the O-terminated surface at one surface of the slab.

B. Thermodynamics

In this section we will give a survey of the thermodynamic formalism which we have used to determine the stability of the structures of the MnO polar terminations in contact with the gas phase. A comprehensive description of this formalism and its former applications can be found elsewhere.[58,59] The thermodynamic quantity which controls the thermal equilibrium between a particle reservoir and the surface is the surface energy γ. At temperature *T* and pressure *p* it is defined by

$$\gamma(T,p)=\left[G(T,p,\{n_x\})-\sum_i n_x\mu_x(T,p_x)\right]/A \qquad (1)$$

in which *G* is the Gibbs free energy of the solid substrate terminated with the surface of interest, *A* is the surface area of the two-dimensional (2D) unit cell, n_x is the number of particles *x* in the solid, and μ_x and p_x are the chemical potentials and the partial pressures of the various species in the gas phase. In the case of MnO(111) we have to consider the three chemical species x=Mn, O, and H. For simplicity we assume the following approximations: (i) zero-point vibrations, vibrational entropy contributions, and enthalpy changes are neglected; (ii) the Gibbs free energy is approximated by the DFT total energies $E(n_x)$. Since all the studied models have an identical substrate with the same number of hydrogen atoms we will refer all DFT total energies to the quantity $n_H\mu_H$, with $n_H=4$ and $\mu_H=\frac{1}{2}E_{H_2}=-3.39$ eV; (iii) we impose that the surface is always in thermal equilibrium with bulk MnO which results in the condition

$$\mu_{\mathrm{Mn}} + \mu_{\mathrm{O}} = E_{\mathrm{MnO}}, \tag{2}$$

in which E_{MnO} is the DFT total energy of MnO. By eliminating μ_{MnO} Eq. (1) takes the form

$$\gamma(T,p) = [E(n_x) - n_{\mathrm{Mn}}E_{\mathrm{MnO}} - (n_{\mathrm{O}} - n_{\mathrm{Mn}})\mu_{\mathrm{O}}]/A. \tag{3}$$

Now, the search for the most stable surface would require the unconstrained minimization of the surface energy, which is not a feasible job. An alternative way is to calculate γ as a function of the chemical potential μ_{O} for all considered surface reconstructions. For a given value of μ_{O} the model with the lowest surface free energy is then the thermodynamically stable phase. The chemical potential can be related to the partial oxygen pressure by

$$\mu_{\mathrm{O}}(T,p) = \mu_{\mathrm{O}}(T,p^0) + 1/2k_BT\ln(p/p^0). \tag{4}$$

For the standard pressure, $p^0 = 1$ atm, the values of $\mu_{\mathrm{O}}(T,p^0)$ have been tabulated in Ref. 62. Thus, γ depending on $\mu_{\mathrm{O}}(T,p)$ can now be converted into a pressure (temperature) dependent function at a fixed temperature (pressure), which allows an easier physical interpretation of the results.

Finally, we need to determine reasonable variational ranges for the chemical potentials. In the present work all energies and chemical potentials are referred to $\frac{1}{2}E_{\mathrm{O}_2}$. The upper bounds for μ_{O} and μ_{Mn} are determined by the assumption that O_2 molecules do not condensate and metallic Mn does not crystallize on the surface, which means that the chemical potentials must be smaller than the total energy of the isolated molecules E_{O_2} and of the bulk $E_{\alpha\text{-Mn}}$

$$\mu_{\mathrm{O}} < 0, \quad \text{and} \quad \mu_{\mathrm{Mn}} < E_{\alpha\text{-Mn}}. \tag{5}$$

Eliminating μ_{Mn} and considering Eq. (2) provides the relation

$$E_{\mathrm{MnO}} - E_{\alpha\text{-Mn}} < \mu_{\mathrm{O}}. \tag{6}$$

The lower bound for μ_{O} is therefore given by the heat of formation of bulk MnO. The evaluation of the heat of formation of bulk MnO would require the total energy of the most stable Mn bulk phase, $E_{\alpha\text{-Mn}}$. Since the crystal structure of the α-Mn ground state is very complicated (with the unit cell containing 58 atoms because the spins are ordered in a noncollinear manner),[63,64] for the energy reference we chose the γ-Mn phase with its simple antiferromagnetic structure. Its energy is denoted as $E_{\gamma\text{-Mn}}$. This is a reasonable choice because Hafner and Hobbs[65] have shown that the energy difference between the α and the γ phase of Mn is 67 meV as derived from VASP calculations with GGA potentials. The PBE and PBE+U energies of formation for MnO (E_f) thus evaluated are listed in Table I together with the DFT total energies of MnO, O_2, and γ-Mn. The PBE+U result of $E_f^{PBE+U} = -4.08$ eV is much lower than the PBE result of $E_f^{PBE} = -2.63$ eV, mainly because the value for γ-Mn is much less negative for the PBE+U case.

As a consequence of the results in Table I we restrict the ranges of the oxygen chemical potential to $-2.63 < \mu_{\mathrm{O}} < 0$ and $-4.08 < \mu_{\mathrm{O}} < 0$, for the PBE and PBE+U derived phase diagrams, respectively.

TABLE I. Calculated PBE and PBE+U energies for the isolated O_2 ($\frac{1}{2}E_{\mathrm{O}_2}$) molecule, and for the bulk phases of Mn ($E_{\gamma\text{-Mn}}$) and MnO (E_{MnO}), and energies of formation of MnO (E_f). All values are given in eV.

	E_{MnO}	$\frac{1}{2}E_{\mathrm{O}_2}$	$E_{\gamma\text{-Mn}}$	E_f
PBE	−16.67	−5.025	−9.011	−2.630
PBE+U	−15.24	−5.025	−6.095	−4.083

III. SURFACE GEOMETRY

In this section we describe the geometrical surface model and the various surface reconstructions considered in our study. The starting geometry is a slab containing 5 layers of pure Mn and 5 layers of pure O atoms according to the sequence Mn-O-Mn. Furthermore, one layer of atomic hydrogen saturates the O-terminated surface on one side of the slab, whereas the other surface is terminated by a pure Mn layer. To avoid artificial surface-surface interactions we consider 9 layers of vacuum. The unreconstructed two dimensional unit cell of the (111) rocksalt surface is hexagonal with a vertical ABC stacking sequence. We maintain the magnetic structure of bulk MnO: in plane the Mn magnetic moments are ferromagnetically aligned whereas the interlayer magnetic ordering is antiferromagnetic. With this setup we allow a global relaxation of the atomic coordinates. The first 5 layers of the H-terminated face of the resulting optimized structure (one hydrogen layer and two layers of Mn and two layers of O atoms) are then chosen as common substrate for the considered reconstructions.

In the following we will discuss the geometry of all surface structures considered, which are depicted in Fig. 1.

(a) *Octopolar*: first proposed by Wolf[45] for the polar MgO(111) surface, the octopolar reconstruction is a pyramid-like structure obtained by removing one quarter of atoms from the subsurface and three quarters of atoms from the surface layer. It consists of either O or Mn triangular based pyramid with O_1-Mn_3-O_4 and Mn_1-O_3-Mn_4 stoichiometry, respectively.

(b) *Spinel*: very similar to the octopolar model, the spinel reconstruction[11] possesses the same O_1-Mn_3-O_4 and Mn_1-O_3-Mn_4 stacking. The only difference with the octopolar structure is that in the spinel termination the topmost species is right above one of the subsurface atoms.

(c) *Alpha*: with an Mn_3-O_4 (Mn terminated) and O_3-Mn_4 (O terminated) stoichiometry, the α structure is obtained by removing the topmost atom from the octopolar reconstruction. This reconstruction does not formally yield the charge compensation, which is achieved by an anomalous filling of the surface state.[4,66]

(d) 2×1: this is a missing-row type reconstruction obtained by removing every other atom in the outermost layer. The resulting structure possesses an Mn_2-O_4 (Mn terminated) or O_2-Mn_4 (O terminated) stoichiometry.

Other types of reconstructions have been found[5] for MgO(111), which comprise the cyclic ozone molecules, i.e., trimers of O centered over underlying Mg atoms. From this class of models we considered (e) *cyclic ozone-*

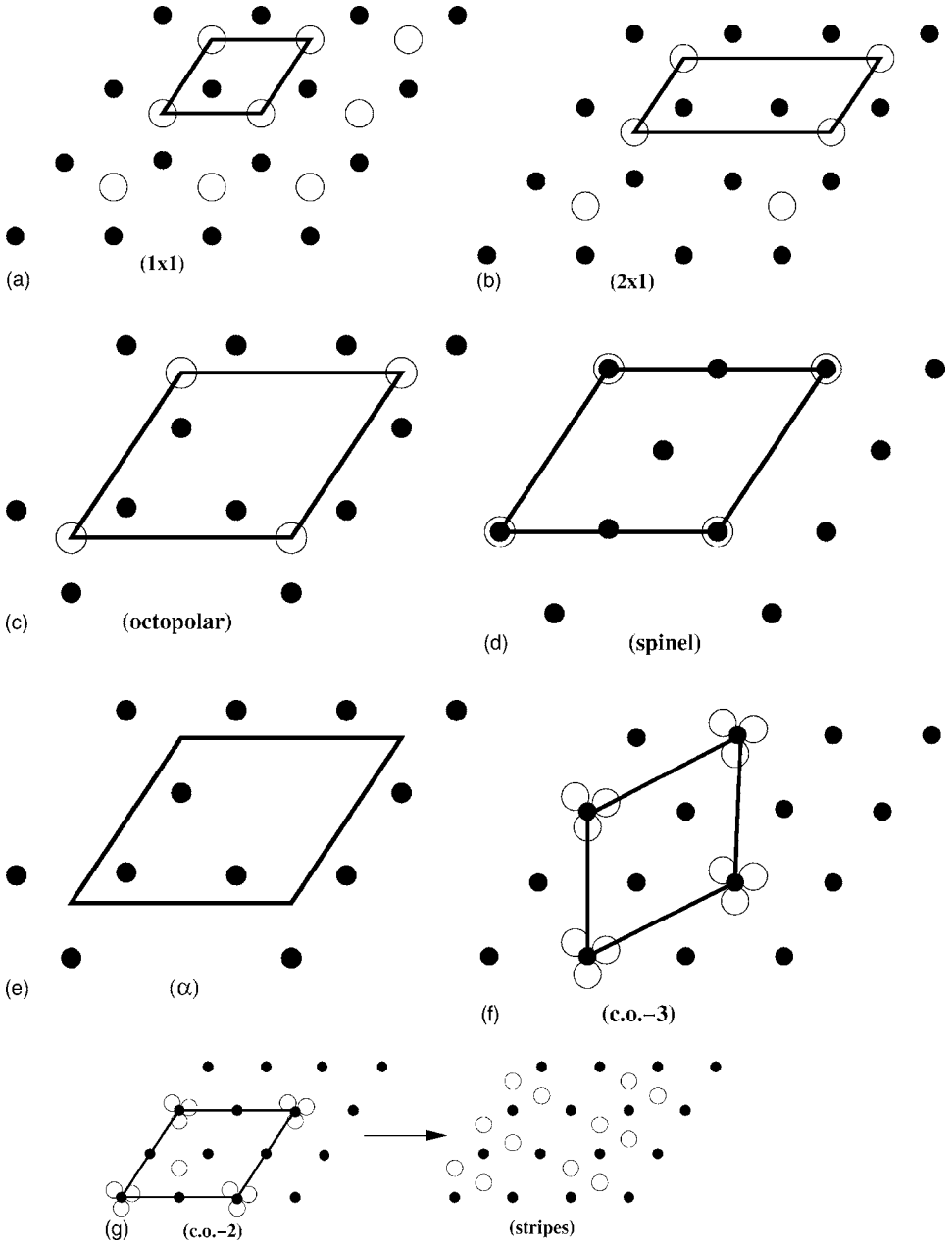

FIG. 1. Top view of geometrical models. Empty circles: O atoms; small filled circles: Mn atoms. Only the O-terminated surfaces are displayed; the Mn-terminated surfaces are obtained by inverting the position of the two types of circles. For the *cyclic ozone* 2×2, the fully optimized structure is also given (*stripes*).

$(\sqrt{3}\times\sqrt{3})R30^\circ$ and (f) *cyclic ozone*-2×2. After a full geometrical relaxation the ozone trimers on top of the *cyclic ozone*-2×2 model dissociate, and the initial structure is converted into a *stripes* structure. Therefore in the following the *cyclic ozone*-2×2 will be indicated as *stripes* structure. We will come back to this point later on. Finally, we propose two more structures derived from the *stripes* surface, by adding additional O atoms in the subsurface layer. The resulting structures, (g) *chain* and (h) *distorted stripes*, contain 1 and 2 extra O atoms in the unit cell, respectively, which we have added to the subsurface of the fully optimized *stripes* structure. None of the former 4 models (e, f, g, and h) fulfill the electrostatic condition for charge neutrality.

IV. RESULTS AND DISCUSSION

In this section we summarize and discuss the results obtained in this study. Although PBE+U should provide a physically more useful description of the electronic and magnetic properties of MnO, the lack of experimental information suggests that both the results of PBE and PBE+U calculations should be discussed. However, we will focus more on the PBE+U results.

Before discussing in more details the geometrical and electronic properties of the most favorable structures we draw some general conclusions on the stability of the various models.

A. Surface phase diagram

To explore whether the MnO(111) termination may lower its surface energy by assuming a reconstructed structure we constructed the surface phase diagram by calculating the surface energies of the models given in Fig. 1, as a function of the actual surface composition being in equilibrium with an

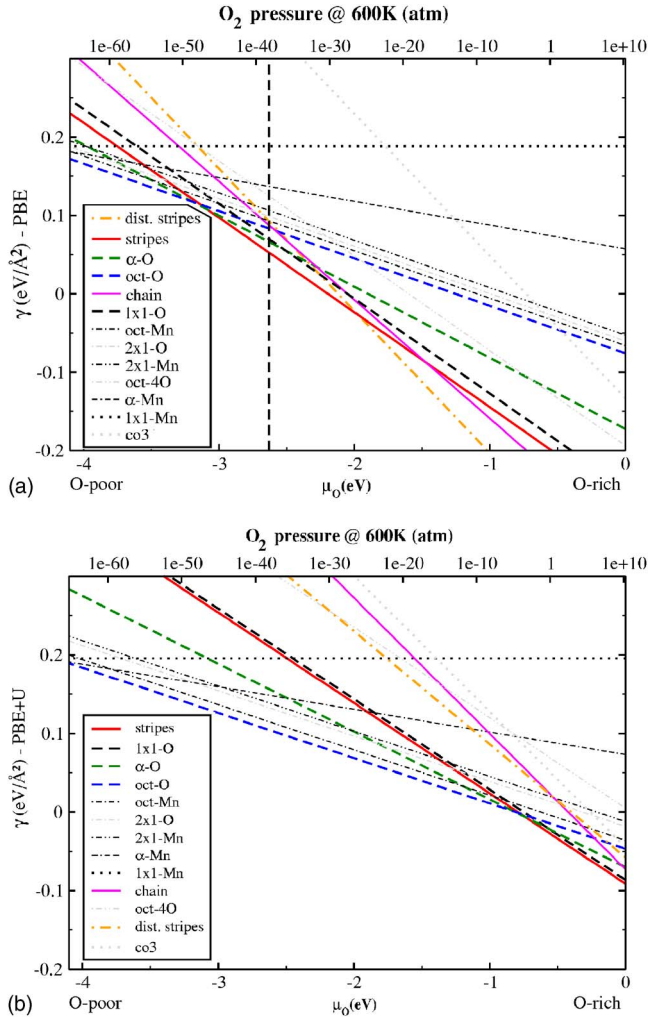

FIG. 2. (Color online) Surface energy γ of the polar MnO(111) surface with different reconstructions as function of the oxygen chemical potential μ_0. Top x axis: pressure scale @ $T=600$ K. Top panel: PBE results, the vertical dashed line indicates the allowed range of μ_0: $-2.63<\mu_0<0$; bottom panel: PBE+U results, for the allowed range of μ_0 is: μ_0: $-4.08<\mu_0<0$.

external oxygen environment, according to Eq. (3). In Fig. 2 we show the results for the MnO(111) reconstructions which have the lowest surface energy, calculated within both the PBE and PBE+U approximation.

We find that within the allowed range of variation of μ_0 the PBE approach predicts two favorable surface structures, namely the *stripes* and the *distorted stripes*. PBE+U, however, yields in the oxygen-rich regime a coexistence between the bulk O-terminated (1×1) surface and the *stripes* structure, for which the surface energies and their slopes are almost degenerate. In a very small interval at $\approx\mu_0=-1$ eV the α-O reconstruction is energetically more favorable, while in the remaining region, i.e., for $-4.08<\mu_0<-1$ the octopolar-O surface becomes the most stable phase. These two structural models, α-O and octopolar-O, are also favored at oxygen-poor condition below -3.0 eV in the PBE phase diagram. However, as indicated by the vertical dashed line in Fig. 2, the values of μ_0 below -2.6 eV exceed the allowed range of the oxygen chemical potential, i.e., for smaller chemical potentials bulk Mn can form. The other surfaces are higher in surface energy for all chemical potentials and will not be formed in thermodynamic equilibrium. Nevertheless, some of the remaining reconstructions are very close in energy to the most stable structure: (i) within PBE, the (1×1)-O and the *chain* structures compete with *stripes* and *distorted stripes* and the octopolar-O surface turns out to be almost degenerate with (2×1)-O, (2×1)-Mn, and octopolar-Mn. The other structures, i.e., α-Mn, (1×1)-Mn, *cyclic ozone*-$(\sqrt{3}\times\sqrt{3})R30°$ and octopolar-4O (an octopolar reconstruction formed by a 4 oxygen pyramid) are less stable surfaces. (ii) Also within PBE+U the (2×1)-O, (2×1)-Mn, and octopolar-Mn surfaces are almost degenerate with the octopolar-O structures being stable over a wide range of the oxygen chemical potential, while in the oxygen-poor regime the α-Mn surface comes closer to the octopolar-O reconstruction. The other models, octopolar-4O, *cyclic ozone*-$(\sqrt{3}\times\sqrt{3})R30°$, *chain* and *distorted stripes* have much too high surface energies and compete in stability with the (1×1)-O and *stripes* structures only in the very oxygen-rich regime, near 0 eV.

Some important issues should be emphasized at this point. The phase diagram discussed so far gives information on the relative stability of different reconstructions over the allowed range of the chemical potential. Since we are limited to a finite set of surface models, others could in principle exist with a lower surface energy. Furthermore, the lack of experimental data and the very large number of degrees of freedom of the system place our *ab initio* investigation at a purely predictive level, which is very difficult to perform for a complex system. Finally, it is important to underline that the models presented in Fig. 1 represent only the initial ideal geometries which have been completely relaxed under the conditions described in Sec. II. Therefore, in some cases the final optimized structure is very different from the starting geometry, as already mentioned for the *cyclic ozone*-2×2 model. Another example is the spinel structure, which we found to be metastable in the sense that after the relaxation the final structure is nothing but the octopolar configuration; i.e., the topmost atom placed right above the subsurface species shifts towards the octopolar hollow site to form the pyramid termination.

B. Structural properties

In this section we present the results obtained for the most stable surface geometries as shown above. We start by comparing the octopolar and the α reconstructions. Later on the *stripes* and their derived (*distorted stripes* structures and the *chain*) reconstructions will be discussed.

1. The octopolar and α surfaces

Figure 3 shows the optimized O-terminated octopolar and α surface structures. Since PBE and PBE+U calculations result in qualitatively similar geometrical results, only the PBE+U relaxed surfaces are represented. We recall that the O-terminated α configuration is obtained by removing the topmost Mn atom from the Mn-terminated octopolar surface.

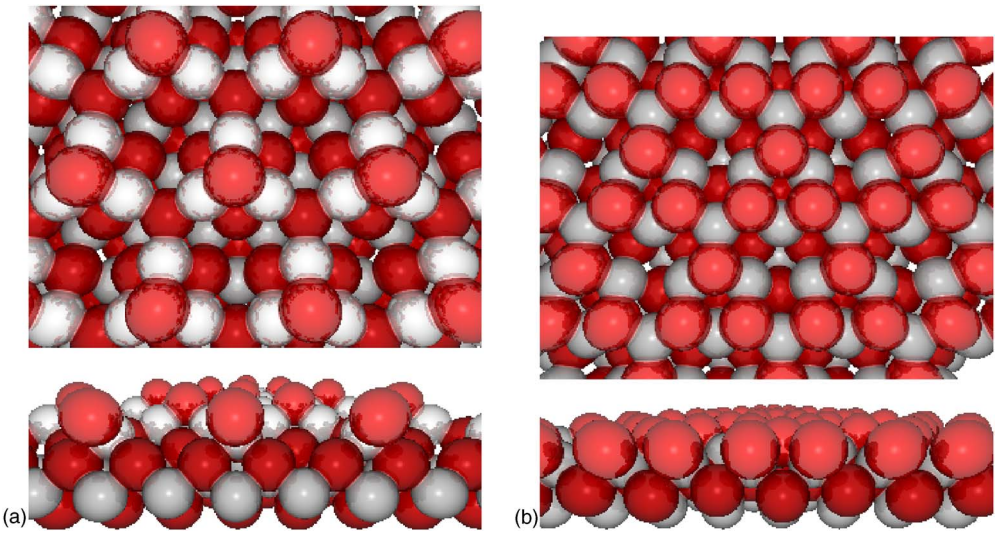

FIG. 3. (Color online) Side (bottom) and top views (top) of the O terminated octopolar (a) and α (b) optimized surface geometries as calculated within the PBE+U approach. Black (Red) balls: O atoms, white balls: Mn atoms. The corresponding Mn terminations is derived by exchanging the atom types.

We focus now on the structures obtained after relaxation. In Table II we report the optimized structures in terms of interlayer distances (d), bucklings (b), and bond lengths (l) between the atomic species forming the triangular basis of the octopolar pyramid and the α structure. For a direct comparison of the octopolar and α data we maintain the same labels for both structures, i.e., in the α model the missing apex atoms are counted as the first layer, and the formal termination becomes the second layer, which can be thus associated with the octopolar pyramid's base. Large relaxations occur for both reconstructions, mainly localized in the topmost 4 layers. Although PBE and PBE+U calculations provide qualitatively similar optimized geometries, within PBE the changes are much larger. In all cases, inward relaxation is found mainly for the first 4 layers, while a bulk-like configuration is maintained in deeper layers, for which the interlayer distances differ from the bulk geometry by only $\sim 1\%$ and also buckling is almost absent. We recall that the geometry of the remaining deeper layers is kept fixed during relaxation. We note that the bond length l always decreases, namely the three atoms in the second layer move towards each other inducing a pyramidal narrowing in the octopolar structure (associated with the inward movement of the apical atom). We also note a reduction of the size of the hole formed by the surface triangles in the α configuration. As a consequence, of this surface shrinking, a very large buckling in the third layer is induced which accommodates the relaxations above. The relaxation along the surface normal decays smoothly to zero in the sixth layer. The only exception is the O-terminated α PBE-optimized structure for which a residual buckling of 0.1 Å remains in the sixth layer. This motion accommodates the enormous relaxations obtained for α-O, as calculated in particular by the PBE approach.

2. The stripes surfaces

The optimized structures of the *stripes*, *distorted stripes*, and *chain* structures are plotted in Fig. 4. As for the models presented above we show only the final PBE+U derived geometries, because the PBE results are qualitatively similar. The quantitative differences are collected in Table III.

The structural change induced by the relaxation of the *cyclic ozone*-2×2 structure is very large. The main structural feature of the ideal starting configuration, depicted in Fig. 1, is the presence of oxygen trimers (cyclic ozone molecules) bonded to the subsurface Mn and connected by additional O atoms placed near the vertices of the trimers. The final optimized geometry drawn in Fig. 4 (top panel) displays a very different structure. It is characterized by wide stripes of oxygen dimers linked by intercalated Mn atoms. The 2D building block is a rectangle formed by four O atoms and one Mn atom placed in the central hollow site. The distance between parallel stripes amount to ≈ 6 Å. The *stripes* model derived from the *c.o.*-2×2 configuration is stoichiometrically equivalent to the bulk O-terminated surface. Although the (1×1)-O termination does not undergo any reconstruction, the PBE+U approach yields these two structures almost degenerate in energy (see Fig. 2). In essence, at very high oxygen pressures, for $\mu_O > -0.8$ eV, the stripes and the unreconstructed (1×1)-O terminations may coexist. The full relaxation of the (1×1)-O surface is also given in Table III.

By adding one O atom in the subsurface of the stripes model we obtain a nearly one dimensional structure as shown in the bottom panel of Fig. 4. These one dimensional features, formed by linear buckled Mn-O-Mn chains, are weakly only bonded to the substrate and separated by ≈ 6 Å. Although this structure is never more stable than others for any oxygen chemical potential, in the oxygen-rich regime it can compete in energy with the most stable surfaces, *stripes*, *distorted stripes*, and (1×1)-O.

Finally, we have placed two additional O atoms into the substrate of the *stripes* model. The resulting structure is the *distorted stripes* model depicted in the top right panel of Fig. 4. As discussed before, the PBE approach favors this structural configuration for $\mu_0 < -1.2$ eV, whereas within the

TABLE II. The structure of the O-terminated octopolar and α reconstructed surfaces, calculated using PBE (top) and PBE+U (bottom). All distances are given in Å, whereas the changes with respect to the bulk values (in brackets) are given in percent relative to the bulk spacings. The symbols are explained in the text.

	oct-O	oct-Mn	α-O	α-Mn
		PBE		
l	2.896 (−6.3)	2.931 (−5.1)	2.819 (−8.8)	2.757 (−10.8)
d_{12}	1.019 (−19.3)	0.928 (−26.5)		
b_2				
d_{23}	1.117 (−11.5)	0.968 (−23.3)	0.707 (−44.0)	1.096 (−13.2)
b_3	+0.594	+0.435	+0.630	+0.551
d_{34}	1.292 (+2.4)	1.357 (+7.5)	1.377 (+6.5)	1.289 (−0.3)
b_4	−0.174	−0.155	−0.376	−0.272
d_{45}	1.279 (+1.3)	1.251 (−0.9)	1.273 (+0.9)	1.283 (+1.7)
b_5	−0.061	−0.143	−0.139	−0.034
d_{56}	1.276 (+1.1)	1.283 (+1.7)	1.277 (+1.2)	1.286 (+1.9)
b_6	−0.037	0.076	−0.129	−0.042
		PBE+U		
l	2.909 (−8.1)	2.982 (−5.8)	2.983 (−5.8)	2.909 (−8.1)
d_{12}	1.133 (−12.3)	1.017 (−21.3)		
b_2				
d_{23}	1.126 (−12.9)	1.145 (−11.4)	0.849 (−34.3)	1.141 (−11.8)
b_3	+0.629	+0.507	+0.447	+0.409
d_{34}	1.351 (+4.5)	1.328 (+2.7)	1.328 (+2.7)	1.323 (+2.3)
b_4	−0.131	−0.148	−0.254	−0.151
d_{45}	1.292 (−0.1)	1.292 (−0.1)	1.315 (+1.7)	1.292 (−0.1)
b_5	−0.048	−0.023	−0.031	−0.020
d_{56}	1.308 (+1.2)	1.291 (−0.2)	1.285 (−0.6)	1.312 (+1.5)
b_6	0.009	0.020	0.063	−0.010
		Bulk		
		Expt.	PBE	PBE+U
l		3.140	3.090	3.167
d		1.283	1.262	1.293

PBE+U approach the *distorted stripes* model gains stability only in the very oxygen-rich region, near $\mu_0=0$, comparable to the *chain* structure.

Now we focus on the quantitative structural aspects of the *stripes* and *chain* reconstructions. First we note that the rectangular building blocks of the stripes remain unchanged in the *stripes* and *distorted stripes* models. This corresponds to $\approx 3\times 4$ Å atomic arrangement with an average O-Mn bondlength of about 2.5 Å. The main differences between the two stripes models are: (i) the size of the vertical buckling in the first layer, which is almost zero in the *stripes* structure ($b_1 \approx 0.15$ Å), gets larger than 1 Å in the *distorted stripes* model ($b_1 \approx 1.23$ Å); and (ii) the structure of the substrate maintains the bulk stacking in the *stripes* surface, whereas in the *distorted* model strong deviations are observed which compensate the strong surface buckling. In the *stripes* surface the formation of the stripes causes an upward movement of two subsurface Mn atoms. The surface structure can therefore be thought of as a "single" layer which is bonded to the substrate via the bonding of two Mn atoms laying in the subsurface interface. Starting from the third layer, the sequence and stoichiometry of the layers is reverted to that of the bulk. A different behavior is found for the *distorted* surface. In this case the outward movement of the subsurface Mn atoms is compensated by the introduction of two additional O atoms. As a consequence, the atoms in the substrate experience a remarkable rearrangement which is characterized by the formation of layers containing 50% Mn and 50% O (*AB-AB-AB* stacking). This reorganization extends to deeper layers; it stops only in the seventh layer, where the bulk fcc *ABC* stacking is reformed.

Finally, a closer look at the chain model (bottom panel of Fig. 4) shows that the superficial Mn-O-Mn rows display an average intrachain Mn-O bond length of about 1.8 Å, and a very large buckling of ≈1.3 Å. The distance between parallel chains is very large, namely ≈6.2 Å, and they are more than 2 Å above the substrate layer. Therefore, the Mn-O-Mn rows can be considered as a corrugated quasi-one-

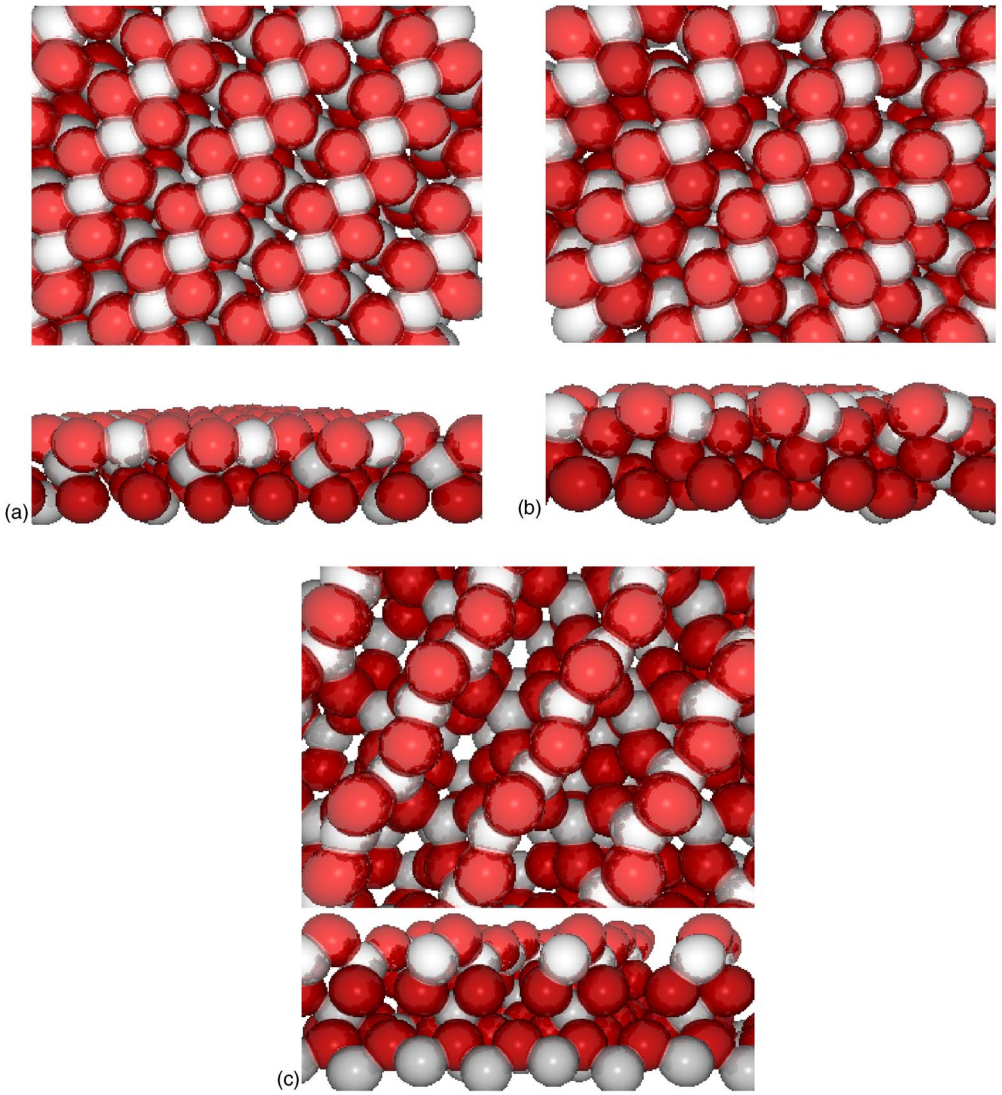

FIG. 4. (Color online) Models of the optimized *stripes* (a), *distorted stripes* (b), and *chain* (c) structures. Side (bottom) and top (top) views of the slab are drawn. Mn and O atoms are represented by white and black (red) spheres, respectively.

dimensional system weakly interacting with the underlying layers. As discussed above, this surface geometry represents a possible metastable structure which can compete in energy with other reconstructions only at extreme oxygen partial pressures. The building process of this chain model is the following: the additional O placed into the substrate induces the downward movement of two superficial O atoms of the *stripes* structure which participate in the formation of an interface layer connecting the surface rows and the bulk-like substrate containing 60% O and 40% Mn atoms.

C. Electronic and magnetic structure

In this section the calculated electronic and magnetic properties of the most favorable reconstructions are discussed. As a guideline for the discussion, we will start presenting the structures which are found stable at oxygen-rich conditions and then we proceed towards smaller pressures. We emphasize that for all structures the bottom O terminations are saturated with H atoms, therefore charge transfer from one surface of the slab to the other one is inhibited.

Although the bulk terminated surface is found to be among the most stable reconstructions only at a very oxygen-rich regime, in order to analyze the stabilization of MnO(111) it is instructive to start from this *simple* case. In Fig. 5 we present the calculated local density of states (DOS) for the O-terminated unreconstructed surface in the surface layer (S), in the subsurface layer (S-1) and in deeper layers (S-7 and S-8). The latter DOS are compared with the bulk DOS as calculated in Ref. 46. For both the PBE and PBE +U approach, the top layer is of metallic character, mostly arising from the hybridization of the subsurface Mn-t_{2g} states with the surface oxygen p_x and p_y states. The presence of states at the Fermi level decreases by moving inside the slab until the insulating bulk character is restored. At this depth, gaps of sizes equal to bulk MnO are obtained. Besides that, the general shape of the surface O-like DOS differs from the bulk-like structure by the formation of a satellite structure in the unoccupied region. This collection of states arises from the hybridization of the surface states with the subsurface

TABLE III. Optimized geometry of the reconstructed surfaces derived from the *stripes* model together with the optimized (1 $\times$1)-O structure, calculated using the PBE and PBE+U approaches.

	PBE	PBE+U
	stripes	
l_1	3.094	3.183
l_2	3.965	4.035
b_1	0.134	0.171
d_{12}	1.196 (−5.2)	1.254 (−3.0)
b_2	0.019	0.007
d_{23}	1.364 (+8.1)	1.312 (+1.5)
b_3	0.293	0.372
d_{34}	1.058 (−16.2)	1.125 (−13.0)
b_4	0.442	0.307
d_{45}	1.136 (−10.0)	1.330 (+2.9)
b_5	0.103	0.026
d_{56}	1.264 (+0.2)	1.308 (+1.2)
b_6	0.048	0.022
	distorted stripes	
l_1	3.097	3.163
l_2	4.004	4.054
b_1	1.166	1.298
	chain	
c	1.795	1.864
Δc	6.180	6.335
b_1	1.215	1.308
d_{12}	2.199 (+74.2)	2.113 (+63.4)
b_2	1.268	1.314
	(1 $\times$1)-O	
d_{12}	0.728 (−42.3)	0.789 (−61.0)
d_{23}	1.406 (+11.4)	1.350 (+4.4)
d_{34}	1.236 (−2.1)	1.308 (+1.1)
d_{45}	1.290 (+2.2)	1.289 (−0.3)
d_{56}	1.251 (−0.9)	1.301 (+0.6)

minority Mn states, favored by the very large contraction of the first interlayer distance (see Table III) which brings the Mn and O layers very close to each other ($\approx$0.7 Å). A very small magnetic moment is induced on the O atoms (0.02 μ_B and 0.35 μ_B, within PBE and PBE+U, respectively), which are found to be antiferromagnetically coupled with the underlying Mn atoms. As regards the subsurface Mn magnetic moments, the reduced interatomic separation lowers the magnetic moments by about $\approx$9% (PBE+U) and 15% (PBE) with respect to the bulk value. As for the interlayer distances, the values of the magnetic moments on the fourth layer regain the bulk value. In summary, at elevated oxygen pressure the bulk O-terminated MnO(111) surface undergoes very strong structural (very large contractions), electronic (insulator to metal transition), and magnetic (reduction of μ_{Mn}) modifications which are localized in the topmost layers, and which decay smoothly into a bulk-like character deeper in the slab.

We continue by discussing the *stripes* structure which is found to be almost degenerate in energy with the unreconstructed O termination. PBE+U yields that this reconstruction is the most favorable one [together with the (1 $\times$1-O case)] for $\mu_{\mathrm{O}} > -0.8$ eV, whereas PBE places its stability in the oxygen-poorest regime ($-2.6 > \mu_{\mathrm{O}} > -2.2$ eV), although it remains one of the competing reconstructions at very oxygen-rich conditions. The DOS for this phase are reported in Fig. 6. Unlike (1 $\times$1)-O, for the *stripes* structure PBE and PBE+U provide a different picture. Within PBE+U the *stripes* structure does not exhibit metallic character, whereas PBE finds states around the Fermi energy of mixed O-like and Mn-like character. This is due to the well known deficiency of standard DFT approximations (like PBE) in evaluating the band gap of correlated systems. In this case, the splitting between occupied and unoccupied d states is strongly underestimated, which leads to the metallic behavior of the surface. As for the PBE+U findings, the surface band gap is reduced by $\approx$50% with respect to the bulk MnO because of the features of the DOS located at about 1 eV above the Fermi energy. These features arise from p_x and p_y O-like states hybridized with planar Mn-$d_{x^2-y^2}$-like states. The absence of O atoms in the subsurface layer destroys this structure thus increasing the value of the gap and leading to a more bulk-like situation below the surface. Similarly to the (1 $\times$1)-O surface, a reduction of the surface Mn magnetic moment is observed, which is not caused by a big contraction of the first interlayer distance as for the (1 $\times$1)-O surface, but rather by the very large structural change induced by the upward movement of 50% of the Mn subsurface atoms, leading to the formation of the Mn-O stripes structure on the surface. In the PBE+U results the O atoms on the surface exhibit a noteworthy induced magnetic moment of 0.26 μ_B.

As discussed previously, by placing additional O atoms in the subsurface layer of the *stripes* structure we have obtained two more potentially metastable phases, namely the *chain* and *distorted stripes* structures containing one and two extra O atoms, respectively. For these two reconstructions we report only the DOS of the surface, plotted in Fig. 7. Similar to the *stripes* structure, PBE and PBE+U result in a different description of these two reconstructions, that is they find a metallic and insulating nature, respectively. Besides the structural changes already discussed, the most obvious features of the adding further O atoms near the surface is that the PBE calculation increases the DOS at the Fermi level, and therefore the metallic character is enhanced; the PBE +U calculation results in a narrowing of the gap which decreases to a few hundreds of meV. The narrowing is due to the downward shift of the Mn($d_{x^2-y^2}$)-O(p_x,p_y)-like structure in the DOS of the conduction band. As a consequence of the metallization of the surface a substantial depletion of the surface Mn magnetic moment is observed.

Let us now focus on the properties of the renowned octopolar termination, reminding that this reconstruction is found to be the most favorable structure at low oxygen pressure,

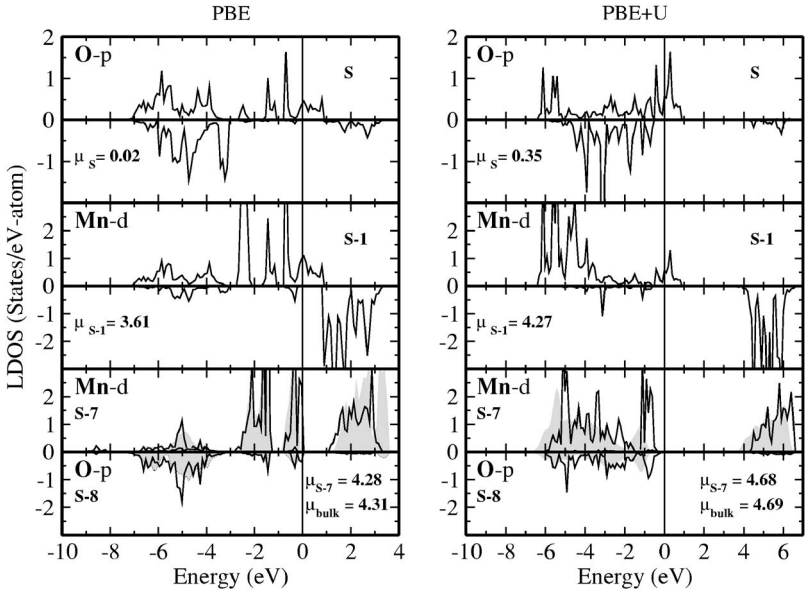

FIG. 5. Layer projected (S=surface, $S-1$ =subsurface) and spin resolved DOS of the O-terminated MnO(111) unreconstructed surface, calculated within the PBE (left panel) and PBE +U approach (right panel). At the bottom, the overlap between the bulk DOS (gray shadow) and the DOS calculated deep in the slab is shown. Energy scale relative to Fermi energy. The values of the Mn magnetic moment (in μ_B) are also reported.

though within PBE its range of stability exceeds the allowed range of μ_O. It is interesting to note that the O- and Mn-terminated octopolar faces are almost degenerate in energy, suggesting that at low oxygen chemical potential the two structures could coexist. We start by discussing the DOS for the O-terminated surface as shown in Fig. 8. (The DOS for the Mn-terminated surface is plotted in Fig. 9.) Both the PBE and the PBE+U approaches derive an insulating ground state for the O-terminated octopolar surface with an energy band gap which is reduced by $\approx$50% with respect to the bulk value. However, the formation of the insulating ground state is different for the two methods. For PBE, the reduction of the band gap is due to the downward shift of the oxygen p-like conduction band states in the surface layer and of the subsurface d Mn states, whereas for PBE+U it is caused by the occurrence of huge oxygen p-like peaks right at the top of the valence band in the surface. The latter process is similar to the reduction of the insulating gap in the O-terminated octopolar NiO(111) surface, as found by an LDA+U approach.[8] Interestingly, the magnetism is only slightly affected by the surface in the PBE+U calculation, in fact only a negligible induced magnetic moment on the topmost O atom is found, and the magnetic moments of the subsurface Mn atoms are almost identical to the bulk value. The situation, however, is different for PBE, for which the magnetic moment of the outermost O atom is significant (0.13 μ_B) and

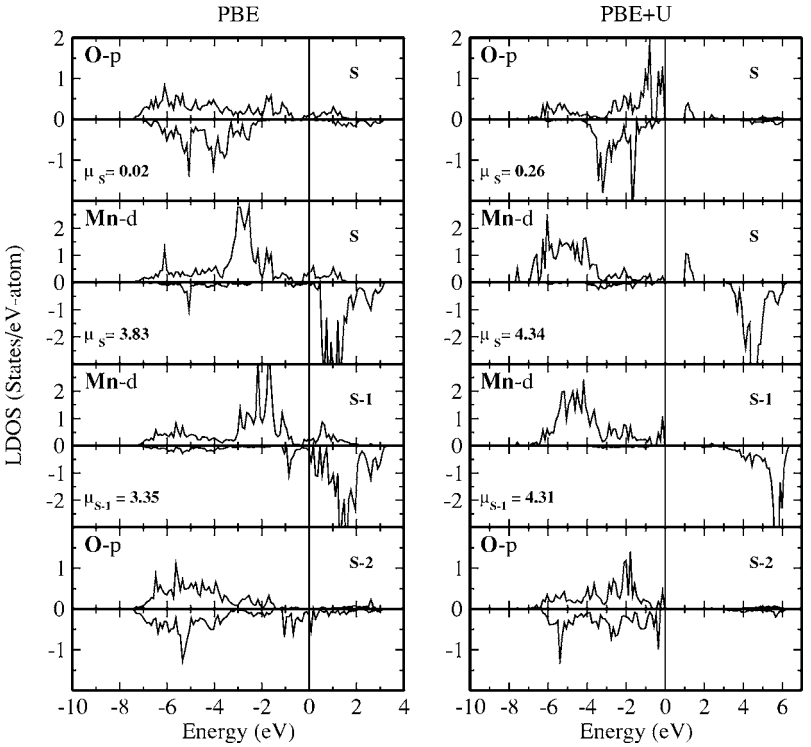

FIG. 6. Spin and layer resolved DOS of the *stripes* structure, calculated within PBE (left panel) and PBE+U (right panel). The two-dimensional surface (S) stripes structure contains four O and two Mn per surface unit cell, whereas the subsurface ($S-1$) is formed by 0.5 monolayers of Mn. For each atom, majority and minority spin states are plotted in different panels. The values of the Mn magnetic moment are also reported (in μ_B).

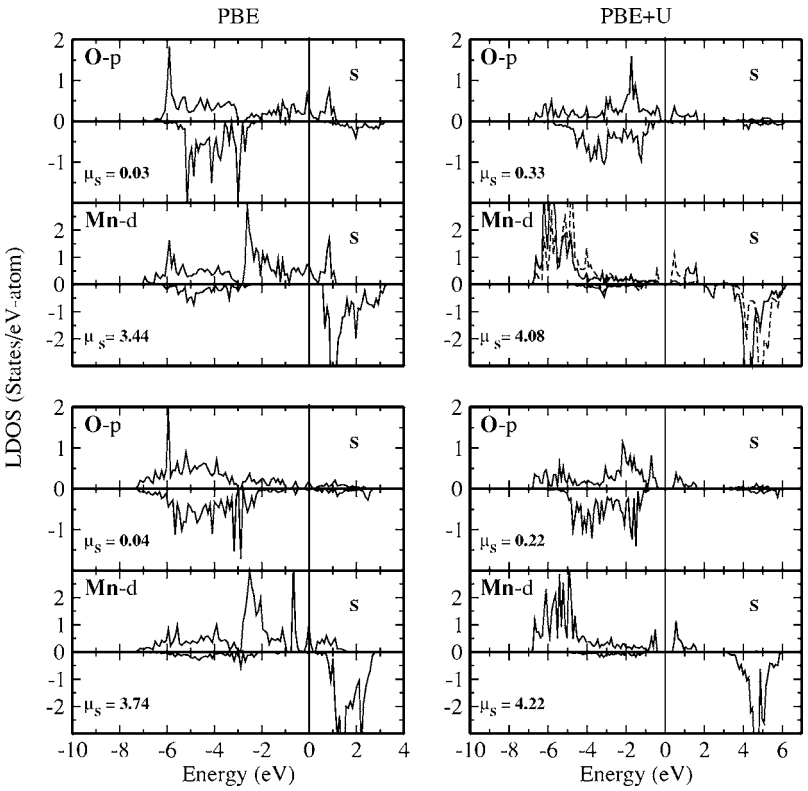

FIG. 7. Spin resolved and layer projected DOS of the *chain* (up) and *distorted stripes* (down) models, calculated within the PBE and PBE+U approaches. Because PBE+U for the *chain* structure results in a different DOS for the two inequivalent surface Mn atoms, both DOS are shown (full and dashed lines).

the magnetic moment of the Mn subsurface atoms is reduced by 2%. The structural changes provoked by the strong inward relaxation (see Table II) affect the first four layers, which display a DOS very different to the bulk. In particular, the buckling in the third and fourth layers modifies the DOS of the inequivalent atoms (dashed lines), namely the atomic species which move away from the layer in order to compensate for the structural rearrangement. Thus, the *p*-like bands of the inequivalent O atoms in the third layer have narrowed and contribute less to the DOS near the Fermi energy. The inequivalent Mn atoms in the fourth layer contribute more to the states on top of the valence band. Starting from the fifth layer, the general electronic and geometrical properties are getting very similar to the bulk.

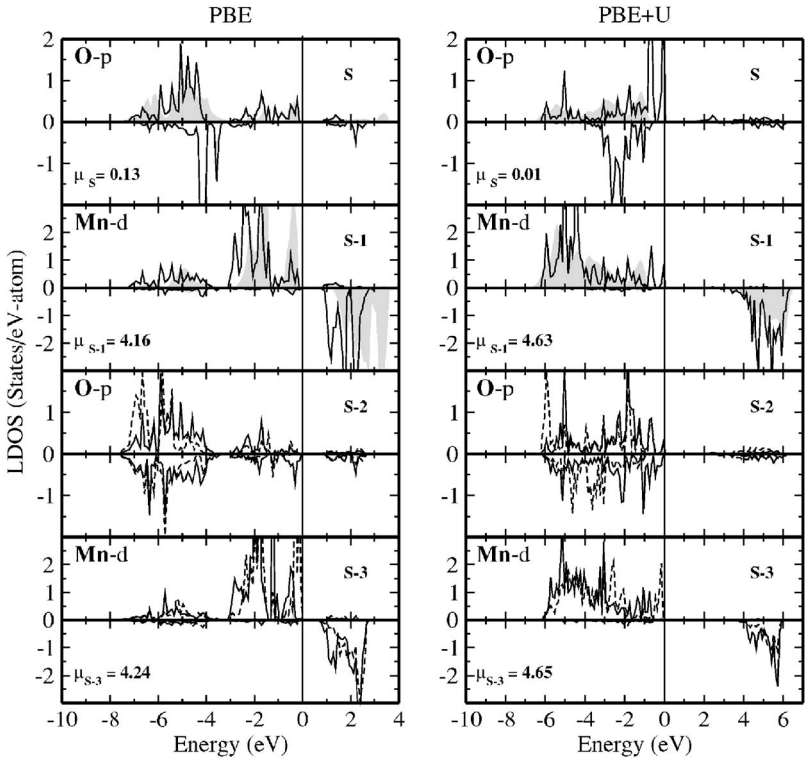

FIG. 8. PBE and PBE+U layer projected and spin dependent DOS of the O-terminated octopolar structure. Gray shadows display the bulk DOS.

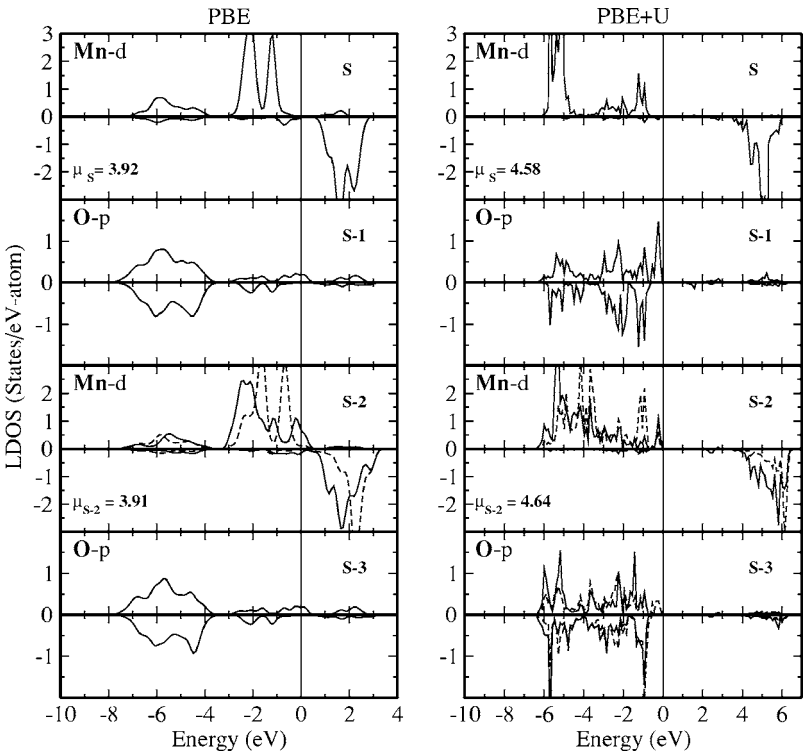

FIG. 9. PBE and PBE+U layer and spin resolved DOS of the Mn-terminated octopolar structure.

Like for the Mn-octopolar termination, again PBE and PBE+U give an opposite description: PBE describes this reconstruction as a quasimetallic surface, caused by the shortening of the distance between minority and majority Mn *d states* and the concomitant broadening of the O-*p*-like bands at the Fermi level. However, the overall DOS at Fermi energy turns out to be very small, but sufficient to destroy the bulk insulating character. Furthermore, a significant depletion of the magnetic moment for the surface Mn atoms is observed. In contrary, within PBE+U this reconstruction gains stability by maintaining an insulating character. However, the presence of O-*p*-like states on top of the valence band at the surface and the appearance of small O and Mn structures a few hundreds meV above the Fermi energy drastically reduce the insulating gap with respect to the bulk value. Similar to the octopolar-O surface, no significant changes in the magnetic structure appears at the surface.

V. CONCLUSIONS

By means of first principles calculations—combining thermodynamic assumptions and DFT total energies—we have carried out an investigation of the surface reconstructions of the polar MnO(111) surface. In the absence of experimental information, we have considered many different surface structures, and for each one the surface energy as a function of the external oxygen chemical potential has been calculated, by using the standard PBE approximation and the PBE+U approach. Though the two methods provide some common conclusions, in particular with respect to the geometrical aspects (Tables II and III), the overall results of the two approaches are somewhat controversial, in particular regarding the metallic/insulating character of the surface and the pressure dependent relative stability of the various models considered. Albeit, the PBE+U approach is expected to be more capable in dealing with correlated systems, such as transition metal oxide AFM insulators like MnO. Therefore we are argue that the conclusions drawn from the application of the PBE+U approach are more relevant than for the PBE results. Accordingly, our final remarks will be drawn following the PBE+U results.

On the basis of energetic and geometrical arguments the existence of some models can be ruled out. The spinel structure after relaxations is changed into an octopolar one, therefore it cannot exist under any pressure conditions. Similarly, all models involving superficial cyclic ozone trimers [*cyclic ozone*-$(\sqrt{3}\times\sqrt{3})R30°$ and *cyclic ozone*-2×2] can be ruled out, since cyclic ozone molecules, upon structural minimization, dissociate and lead to the formation of other surface reconstructions. Inspecting the phase diagram in Fig. 2 one can exclude the formation of other structures, namely the octopolar-4O, (2×1)-Mn, and 2×1-O models, since their surface energies are far too high. Two more structures which are highly improbable are the (1×1)-Mn and the α-Mn terminations, which may compete in energy with more favorable reconstructions only in the very oxygen-poor regime.

The *stripes* structure, derived from the relaxation of the *cyclic ozone*-2×2 model deserves special attention, because in the O-rich regime ($\mu_O > -0.8$ eV) it is found to be the most stable structure together with the unreconstructed (1×1)-O surface. These two reconstructions have the same chemical composition, namely four Mn and four O atoms in the first two layers, but the atomic species are differently placed in the surface. The (1×1)-O termination displays the bulk-like stacking, whereas in the *stripes* structure four O and two Mn atoms lay on the surface which is bridged to the substrate by two subsurface Mn atoms. Starting from the

third layer and deeper, the two slabs differ only by the presence of vertical bucklings in the *stripes* structure. Furthermore and more significantly, these two surfaces are insulating and have very similar DOS, although the presence of a bundle of bands in the conduction states regime of the *stripes* structure notably reduces the band gap. Additional O atoms in the subsurface of the *stripes* model further destabilizes the insulating character and leads to the formation of other two structures, the *chain* and *distorted stripes* structures, which could compete in energy with the above terminations at very high oxygen pressures; interestingly, the *distorted stripes* termination is found to be the most favorable one for $\mu_O > -1.2$ eV within PBE. For $\mu_O \approx -0.8$ eV, we observe a crossing point in the phase diagram where three more phases come to play an important role: the two O-terminated and Mn-terminated octopolar surfaces and the α-O reconstructions. The latter one, obtained by removing the apex Mn atom from the oct-Mn surface, can be considered as a metastable phase, joining the high pressure reconstructions with the octopolar one. By moving towards lower chemical potentials, the octopolar O-terminated surface becomes the most stable reconstruction and remains the most stable structure for the very wide range of the oxygen chemical potential of $-4.1\ \text{eV} > \mu_O > -0.9$ eV. Interestingly, the oct-Mn termination, whose line in the phase diagram displays the same slope as the oct-O one, is found to be only 10 meV less stable than the oct-O surface, suggesting a possible coexistence of both phases in different surface domain. Both structures exhibit an insulating character, though the presence of oxygen satellite structures—common to both terminations—reduces the insulating gap to ≈ 1 eV. Furthermore, these are the only two structures for which the magnetism is almost not affected by the formation of the surface as a result of the competition between exchange interactions and electron mobility: the tendency of the magnetic moment to increase on the surface due to the reduced coordination is compensated by the large contractions of the first two layers inducing a *metallization* of the surface (in the sense of reduced insulating character).

In conclusion, the compensation of polarity in MnO(111) occurs through an interplay between modifications of the surface structure and the drastic changes of the electronic character induced by a general rearrangement of the charge distribution in the topmost layers, which eventually reduce the bulk insulating band gap. As for the interaction with an oxygen reservoir, we have shown that for a wide range of oxygen chemical potential the octopolar reconstruction turns out to be the most favorable phase. However, at very oxygen-rich regimes the so called *stripes* structures, resulting from the dissociation of cyclic ozone molecules on the bulk terminated Mn face, gain in stability and compete in energy with the unreconstructed oxygen termination.

ACKNOWLEDGMENTS

This work was supported by the Austrian Science Fund FWF within the Joint Research Programme S90, the START program Y128, and the Science College W4.

*Also at: INFM-SLACS, Sardinian Laboratory for Computational Materials Science, University of Cagliari, Italy.

[1] G. Renaud, Surf. Sci. Rep. **32**, 1 (1998).
[2] C. Noguera, J. Phys.: Condens. Matter **12**, R367 (2000).
[3] V. K. Lazarov, R. Plass, H. C. Poon, D. K. Saldin, M. Weinert, S. A. Chambers, and M. Gajdardziska-Josifovska, Phys. Rev. B **71**, 115434 (2005).
[4] F. Finocchi, A. Barbier, J. Jupille, and C. Noguera, Phys. Rev. Lett. **92**, 136101 (2004).
[5] R. Plass, K. Egan, C. Collazo-Davila, D. Grozea, E. Landree, L. D. Marks, and M. Gajdardziska-Josifovska, Phys. Rev. Lett. **81**, 4891 (1998).
[6] A. Wander, I. J. Bush, and N. M. Harrison, Phys. Rev. B **68**, 233405 (2003).
[7] J. Goniakowski and C. Noguera, Phys. Rev. B **66**, 085417 (2002).
[8] O. Bengone, M. Alouani, J. Hugel, and P. Blöchl, Comput. Mater. Sci. **24**, 192 (2002).
[9] A. Wander, F. Schedin, P. Steadman, A. Norris, R. McGrath, T. S. Turner, G. Thornton, and N. M. Harrison, Phys. Rev. Lett. **86**, 3811 (2001).
[10] A. Barbier, C. Mocuta, H. Kuhlenbeck, K. F. Peters, B. Richter, and G. Renaud, Phys. Rev. Lett. **84**, 2897 (2000).
[11] A. Barbier, C. Mocuta, and G. Renaud, Phys. Rev. B **62**, 16056 (2000).
[12] J. Goniakowski and C. Noguera, Phys. Rev. B **60**, 16120 (1999).
[13] A. Pojani, F. Finocchi, J. Goniakowski, and C. Noguera, Surf. Sci. **387**, 354 (1997).
[14] D. Cappus, M. Hassel, E. Neuhaus, M. Heber, F. Rohr, and H.-J. Freund, Surf. Sci. **337**, 268 (1995).
[15] O. Dulub, U. Diebold, and G. Kresse, Phys. Rev. Lett. **90**, 016102 (2003).
[16] G. Kresse, O. Dulub, and U. Diebold, Phys. Rev. B **68**, 245409 (2003).
[17] B. Meyer, Phys. Rev. B **69**, 045416 (2004).
[18] F. Bottin, F. Finocchi, and C. Noguera, Phys. Rev. B **68**, 035418 (2003).
[19] V. E. Henrich, Surf. Sci. **57**, 385 (1976).
[20] H. Onishi, C. Egawa, T. Aruga, and Y. Iwasawa, Surf. Sci. **191**, 479 (1987).
[21] R. Plass, J. Feller, and M. Gajdardziska-Josifovska, Surf. Sci. **414**, 26 (1998).
[22] C. R. Henry and H. Poppa, Thin Solid Films **189**, 303 (1990).
[23] M. Tsukada and T. Hoshino, J. Phys. Soc. Jpn. **51**, 2562 (1982).
[24] G. W. Watson, J. Chem. Soc., Faraday Trans. **92**, 433 (1996).
[25] M. Baudin, M. Wojcik, and K. Hermansson, Surf. Sci. **375**, 374 (1997).
[26] K. Hermansson, M. Baudin, B. Ensig, M. Alfredsson, and M. Wojcik, J. Chem. Phys. **109**, 7515 (1998).
[27] S. C. Parker, N. H. de Leeuw, and S. E. Redfern, Faraday Discuss. **114**, 381 (1999).
[28] K. Refson, R. A. Wogelius, D. G. Fraser, M. C. Payne, M. H. Lee,

and V. Milman, Phys. Rev. B **52**, 10823 (1995).
[29] A. Barbier and G. Renaud, Surf. Sci. Lett. **392**, L15 (1997).
[30] A. Barbier, G. Renaud, C. Mocuta, and A. Stierle, Surf. Sci. **433-435**, 716 (1999).
[31] O. L. Warren and P. A. Thei, J. Chem. Phys. **100**, 659 (1994).
[32] F. Rohr, K. Wirth, J. Libuda, D. Cappus, M. Baümer, and H. J. Freund, Surf. Sci. **315**, L977 (1994).
[33] D. Cappus, C. Xu, D. Ehrich, B. Dillmann, C. A. Ventrice, Jr., K. Al-Shamery, H. Kuhlenbeck, and H. J. Freund, Chem. Phys. **177**, 533 (1993).
[34] H. Hannemann, C. A. Ventrice, Jr., T. Bertrams, A. Brodde, and H. Neddermeyer, Phys. Status Solidi B **146**, 289 (1994).
[35] C. A. Ventrice, Jr., T. Bertrams, H. Hannemann, A. Brodde, and H. Neddermeyer, Phys. Rev. B **49**, R5773 (1994).
[36] P. M. Oliver, G. W. Watson, and S. C. Parker, Phys. Rev. B **52**, 5323 (1995).
[37] P. A. Cox and A. A. William, Surf. Sci. **152/153**, 791 (1985).
[38] C. Mocuta, A. Barbier, and G. Renaud, Appl. Surf. Sci. **162/163**, 56 (2000).
[39] M. Hassel and H-J. Freund, Surf. Sci. **325**, 163 (1995).
[40] K. Mori, M. Yamazaki, T. Hiraki, H. Matsuyama, and K. Koike, Phys. Rev. B **72**, 014418 (2005).
[41] K. Koike and T. Furukawa, Phys. Rev. Lett. **77**, 3921 (1996).
[42] Sh. Shaikhutdinov, M. Ritter, and W. Weiss, Phys. Rev. B **62**, 7535 (2000).
[43] W. Ranke, M. Ritter, and W. Weiss, Phys. Rev. B **60**, 1527 (1999).
[44] P. W. Tasker, J. Phys. C **12**, 4977 (1979).
[45] D. Wolf, Phys. Rev. Lett. **68**, 3315 (1992).
[46] C. Franchini, V. Bayer, R. Podloucky, J. Paier, and G. Kresse, Phys. Rev. B **72**, 045132 (2005).
[47] S. Ito, J. Ohta, H. Fujioka, and M. Oshima, Appl. Surf. Sci. **197/198**, 384 (2002).
[48] W. Neubeck, L. Ranno, M. B. Hunt, C. Vettier, and D. Givord, Appl. Surf. Sci. **138/139**, 195 (1999).
[49] G. Parteder, S. Surnev, and F. P. Netzer (unpublished).
[50] G. Kresse and J. Hafner, Phys. Rev. B **48**, 13115 (1993).
[51] G. Kresse and J. Furthmüller, Comput. Mater. Sci. **6**, 15 (1996).
[52] J. P. Perdew, K. Burke, and M. Ernzerhof, Phys. Rev. Lett. **77**, 3865 (1996).
[53] P. E. Blöchl, Phys. Rev. B **50**, 17953 (1994).
[54] G. Kresse and D. Joubert, Phys. Rev. B **59**, 1758 (1999).
[55] M. Imada, A. Fujimori, and Y. Tokura, Rev. Mod. Phys. **70**, 1039 (1998).
[56] V. I. Anisimov, J. Zaanen, and O. K. Andersen, Phys. Rev. B **44**, 943 (1991).
[57] S. L. Dudarev, G. A. Botton, S. Y. Savrasov, C. J. Humphreys, and A. P. Sutton, Phys. Rev. B **57**, 1505 (1998).
[58] M. W. Finnis, Phys. Status Solidi A **166**, 397 (1998).
[59] K. Reuter and M. Scheffler, Phys. Rev. B **65**, 035406 (2002).
[60] E. Kaxiras, Y. Bar-Yam, and J. D. Joannopoulos, Phys. Rev. B **35**, 9625 (1987).
[61] J. Yamauchi, M. Tsukada, S. Watanabe, and O. Sugino, Phys. Rev. B **54**, 5586 (1996).
[62] D. R. Stull and H. Prophet, *JANAF Thermochemical Tables*, 2nd edition (U. S. National Bureau of Standards, Washington, D.C., 1971).
[63] A. J. Bradley and J. Thewlis, Proc. R. Soc. London, Ser. A **115**, 465 (1927).
[64] T. Yamada, N. Kunitomi, Y. Nakai, D. E. Cox, and G. Shirane, J. Phys. Soc. Jpn. **28**, 615 (1970).
[65] J. Hafner and D. Hobbs, Phys. Rev. B **68**, 014408 (2003).
[66] R. F. W. Bader, Chem. Rev. (Washington, D.C.) **91**, 893 (1991).